Nanofabrication via Maskless Localized Atomic Layer Deposition of Patterned Nanoscale Metal Oxide Films

Laabdia Midani, Waël Ben-Yahia, Vincent Salles, Catherine Marichy

Nanofabrication via Maskless Localized Atomic Layer Deposition of Patterned Nanoscale Metal Oxide Films

Laabdia Midani, Waël Ben-Yahia, Vincent Salles, Catherine Marichy*

Laboratoire des Multimatériaux et Interfaces, UMR CNRS 5615, Univ Lyon, Université Claude Bernard Lyon 1, F-69622 Villeurbanne, France.

*Corresponding author: catherine.marichy@univ-lyon1.fr

Abstract: A modified open-air spatial atomic layer deposition (SALD) head is employed to fabricate complex oxide patterns on various substrates. The co-reactant being kept in the surrounding atmosphere, a simple injection head that consists of three concentric nozzles with only one precursor outlet has been designed. Easy and reversible modification in the diameter of the metal precursor outlet permits direct patterning with different lateral sizes. Maskless deposition of uniform and homogenous TiO_2 and ZrO_2 thin films is successfully demonstrated with a lateral resolution tuned from millimeters to hundred micrometers range while keeping a film thickness in the range of a few to hundreds of nanometers with a control at the nanoscale. This localized SALD approach, named LOCALD, also enables layer stacking and deposition on structured substrates.

Keywords: Spatial atomic layer deposition, patterning, thin film, functional materials, area selective deposition, open-air

Nowadays, interest in nanotechnologies is strongly expanded in many domains like nanoelectronics, energy, transportation, medicine and environment. Precise designs of micro- and nanostructures are sought after for many devices and applications such as thin films transistors, diodes, electrocatalysts, solar cells, sensors or membranes. Additive and subtractive technologies are thus areas of extensive research. In particular, additive approaches permit controlled stacking of layers made of different materials. Direct write techniques as ink-based,[1–4] laser transfer,[5,6] thermal spray[7] and beam depositions[8–14] have been widely investigated these last decades. However, they display limitations either in thickness of the deposited material, in lateral resolution or structuring scale. While combining control of at least one dimension at the nanometer level with large scale patterning is challenging in the direct write approach, lithography is a well-established technique for nanopatterning[15–17] that permits high resolution even down to a few of tens nanometer pitch[18] even over a large surface. However, based on multi-steps including etching, it is time and cost-consuming and may damage sensitive material.

Regarding the latter concerns, atomic layer deposition (ALD) appears well-suited as it is a technique to fabricate (ultra) thin film at low temperature with a thickness controlled at the angstrom level. Based on sequential exposure of the substrate to different precursors reacting with the surface in a self-limited manner,[19] it has already proven to be a technique of choice for microelectronics applications[20] and for fabricating complex nano-/hetero-structures.[21,22] Due to its high conformability and accuracy, it has been implemented to nanopatterning, in particular for spacer deposition in multiple patterning, using conventional lithography and lift-off techniques.[23] ALD being based on sequential self-saturated surface reactions, area-selective deposition (ASD) has also been developed using either activation or

deactivation of the surface to favor or inhibit the growth on specific areas. Advantageous self-alignment of the growth is observed, nonetheless, local chemical modification of the surface meaning pre-patterning of the substrate is still required prior to ALD.[24] One of the main challenges is then the fabrication of directly patterned thin films with a precise thickness and lateral dimensions as well as controlled location on the desired substrate, with suitable production speed and gentle conditions like low temperature and atmospheric pressure. In this regard, open-air, high throughput and/or in-line techniques are sought after. Patented in 1977 and 1983 by Suntola[25,26] and relying on the same principle as ALD, spatial atomic layer deposition (SALD) has attracted a lot of interest since the last decade as it might increase the production speed, be roll-to-roll compatible and also even performed in atmospheric pressure.[27–29] Indeed, while conventional ALD, also called temporal ALD, involves the separation of the precursors in time using successive reactant pulse and purge steps, SALD relies on spatial separation of the reactants. The precursors are continuously delivered in different locations, separated by inert/exhaust areas that prevent the gas reactions. By moving the substrate from an area to another, an ALD cycle (exposition to precursor A, purge, exposition to precursor B, purge) is reproduced.[30] Different types of reactors have been reported.[30–32] They can be operated either under vacuum[33–35] or at atmospheric pressure[36,37] and can involve either translation or rotation displacement. In particular, Levy *et al.*[38,39] developed a reactor geometry based on a close-proximity head that presents the advantage to be operated in open-air.[29,40] To avoid precursors intermixing, typically a space of 50-200 µm between the head and the substrate is fixed,[28,41] leading to the formation of gas-bearing instead of a gas shield.[30] Thus a short distance between the different precursor zones can be set allowing a smaller design of open-air reactors than “conventional” ones. Operating in open-air permits also to get rid of vacuum and/or purge step during sample loading, which is advantageous for roll-to-roll process integration.[36,40] Plasma activation has also been implemented in reactors.[42,43] SALD technique demonstrates strong potential as in photovoltaic[31,40,44–47] and microelectronic domains.[30,48] It also allows fabricating patterned thin film devices either by lithography approach or when combined with ASD.[49] For instance, polymer patterns deposited using inkjet printing with a maximum lateral resolution of 70-90 µm are used as inhibitors for the subsequent SALD of thin film transistors.[31,49–51]

Unlike temporal ALD, direct patterning can also be achieved by this technique as has already been reported a few times.[42,52–54] Plasma-enhanced SALD enables direct deposition of thin film patterns by localization of the plasma on specific areas, with no growth being observed without plasma exposure. For instance, Al_2O_3 circular patterns with millimeter lateral resolution have been demonstrated using switched localized atmospheric pressure plasma source.[42] Complex TiO_2 shapes have also been successfully deposited from N_2/O_2 microplasma printer.[52] In 2019, Masse de la Huerta *et al.*[54] demonstrated that controlled reactant intermixing in open-air close-proximity SALD can be used to perform localized deposition of stripes by careful tuning of the substrate-head gap. Later on, the same group developed customized close-proximity SALD heads, which are fabricated by additive manufacturing, and in particular a cylindrical head consisting of concentric gas outlets. Direct printing of complex patterns with a lateral resolution of several millimeters is successfully demonstrated using this so-called SALD pen.[53] Nonetheless exchanging the head appears necessary to access different ranges of lateral resolution. It should be mentioned that ATLANT3D™ nanosystem company also reports direct patterning with a similar approach.

Direct conformal film patterning with a thickness control at the nanometer level and lateral resolution at micrometer even millimeter range will certainly permit heterogeneous integration of different materials with miscellaneous functions as optoelectronics and piezoelectricity. Combining patterns with complementary properties paves the way to applications such as power electronics, microfluidic, advanced optics (microlenses) or gas sensing.

In the present work, a simple versatile miniaturized open-air SALD head that consists of three concentric nozzles (Figure 1) has been designed for maskless localized deposition of TiO_2 and ZrO_2 thin film patterns with z resolution at the nanoscale. The SALD injection head consists of a triaxial nozzle with an outlet for a single precursor (Figure 1). The surrounding atmosphere is employed as a co-reactant, *i.e.* water from relative humidity in this work. The impact of atmospheric water on Al_2O_3 growth using SALD web coating reactor has been previously reported.[55] Based on the ALD principle, deposits of tens to hundreds of nanometers are reported here. Lateral resolution can be controlled in the range of millimeters to micrometers by reversibly inserting a glass capillary into the central outlet to tune its diameter. SALD characteristics and influence of the SALD parameters are studied. Deposition on various planar and structured substrates is also investigated. Complex and multilayer oxide patterns are successfully deposited using the proposed approach.

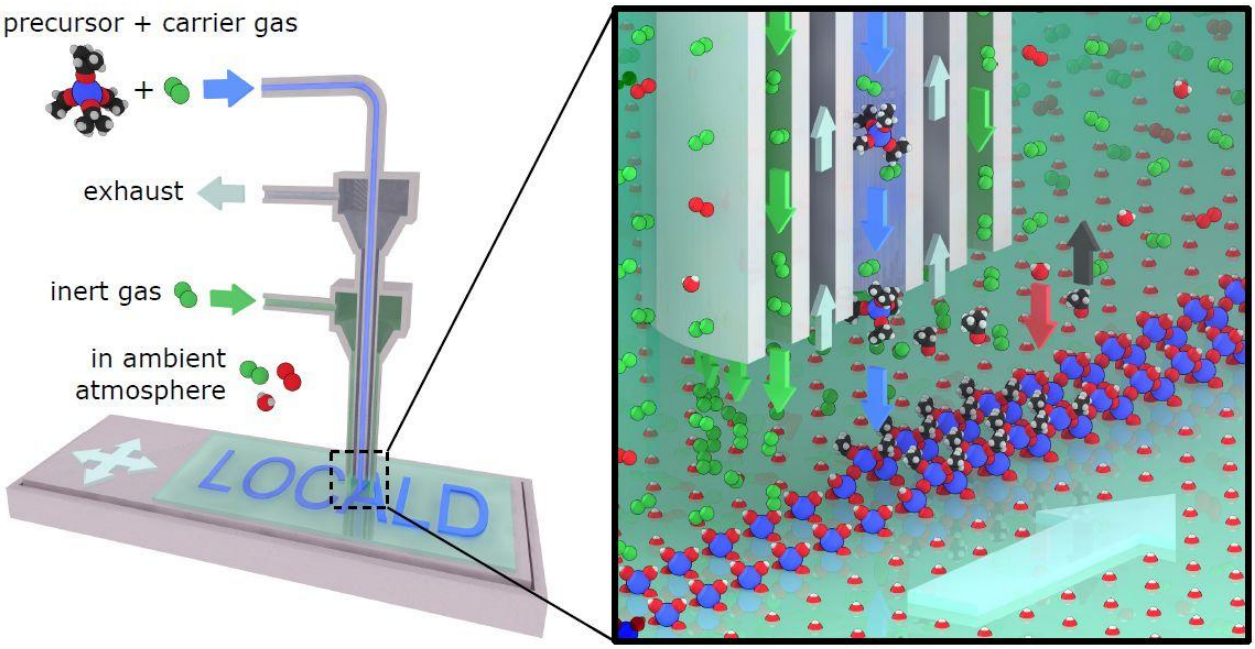

Figure 1. Scheme of the open-air spatial ALD reactor, called LOCALD. Its principle that permits direct local deposition is depicted in the case of TiO_2. The cyan arrow depicts the movement of the substrate, responsible for the different precursor exposures.

Results and discussion

Titanium (TiO_2) and zirconium oxides (ZrO_2) are successfully deposited at 150 °C in a controlled manner using a homemade open-air close-proximity SALD system, which permits using a simple small injection head made of a triaxial nozzle and the surrounding atmosphere as co-reactant. Saturated growth, at 150

°C, is obtained with optimized N_2 carrier- and N_2 purging/protective-gas fluxes (Figure S1 in Supporting information, SI). The substrate-head distance (TiO_2: 300 µm – ZrO_2: 150 µm), the exhaust speed (800 sccm) and substrate velocity (20 $mm.s^{-1}$) are kept constant. To ensure effective separation between the metallic precursor and the surrounding atmosphere, fluxes of N_2 purging/protective gas and N_2 carrier gas are set at 75 sccm (15 sccm) and 25 sccm (15-25 sccm), respectively, for TiO_2 (ZrO_2) deposition. No growth is observed in static mode, i.e. without substrate displacement. Linear dependence of the film thickness on the number of cycles is also evidenced in Figure 2. The determined growths per cycle (GPC) are 0.75 Å/cycle and 2.1 Å/cycle for TiO_2 and ZrO_2, respectively. These values are consistent with a self-limiting process and close to reported ones in the literature for TiO_2[56–58] and ZrO_2[59–61] temporal ALD. A GPC of 0.35 Å/cycle has been previously observed at 120°C using TiO_2 SALD on polyethylene naphtalate.[43] Regarding ZrO_2, any process using Zirconium tert-butoxide and water has been reported so far to our knowledge.

The thickness of the deposit from a few to hundreds of nanometers is thus simply controlled by the number of SALD cycles with accuracy at the nanoscale. For instance, 150 SALD cycles lead to a 10.2 ± 0.6 nm thick TiO_2 film. In the following for ease of characterization, a minimum thickness of 20 nm will be targeted.

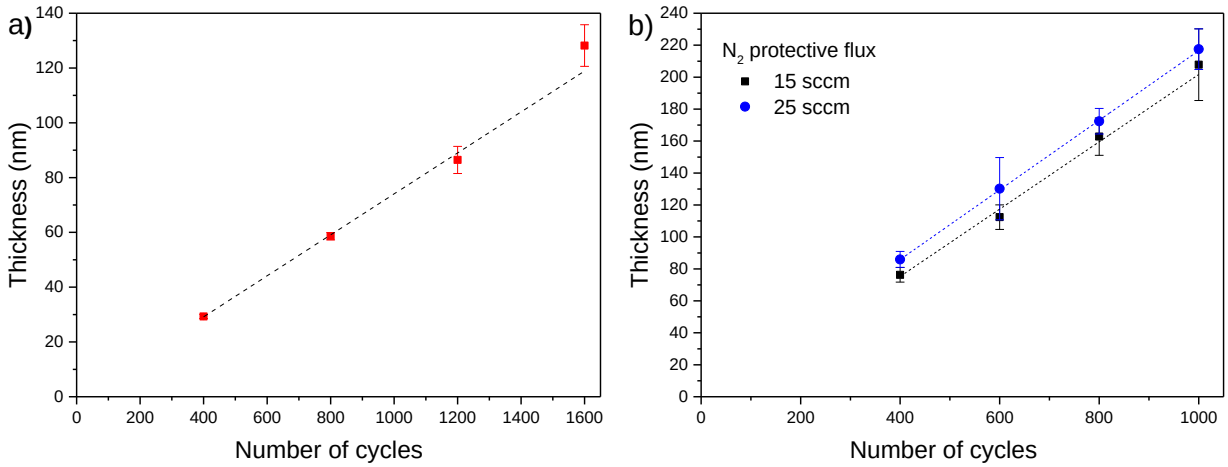

Figure 2. Thicknesses of a) TiO_2 and b) ZrO_2 lines on Si wafer as a function of the number of SALD cycles. Dotted lines correspond to the linear fits. Their slop corresponds to the GPC.

Characteristics of the injection head used allow miniaturizing and localizing the deposit without any pre-treatment of the substrate. TiO_2 and ZrO_2 are then successfully deposited on various supports such as Si wafer, titanium, aluminium and copper foils, TA6V alloy, glass slides and sapphire, in a controlled manner in terms of thickness, shape, dimensions and positioning. Figure 3 displays different TiO_2 and ZrO_2 patterns achieved with a lateral resolution in the millimeter range. The latter is restricted by the diameter of the precursor outlet. Good thickness homogeneity is observed along the pattern as verified by ellipsometry (Figure 3f). One should notice that the thickness at the line extremities is half than that of the deposit, in agreement with a controlled process without air/metal precursor mixing. Indeed, both ends undergo half of the performed cycles. At the opposite, crossings are thicker as expected (Figure 3).

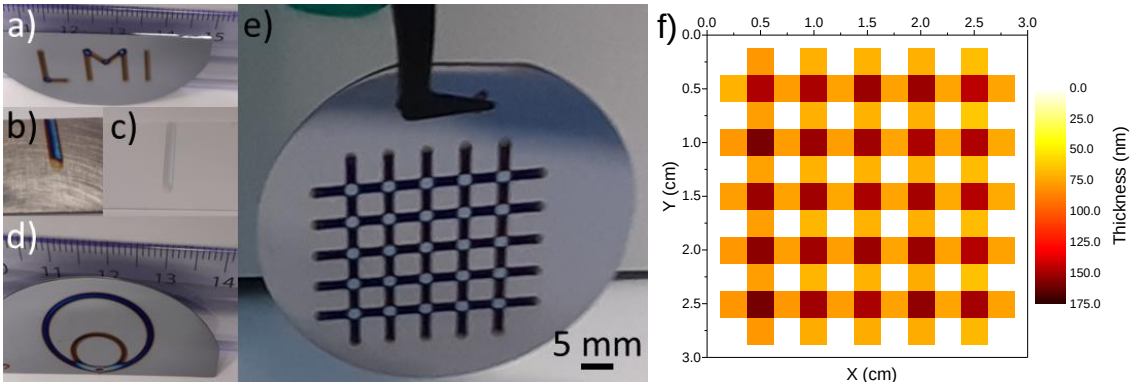

Figure 3. Photographs of TiO_2 patterns deposited on a) Si wafer, b) aluminum alloy and c) glass slide after 600, 500 and 800 SALD cycles, respectively. Photographs of ZrO_2 locally deposited on 2" Si wafers with different patterns: d) circles (400 and 300 cycles), e) grid (1000 cycles) and f) its corresponding thickness map realized by ellipsometry. One measurement is recorded from each section of the grid. No measurement was recorded between lines and at their extremities.

At the chosen deposition temperature, TiO_2 and ZrO_2 are amorphous and smooth (Figure S2). In Figure 4a, the energy-dispersive X-ray spectroscopy (EDS) profile recorded at 6 kV evidences the deposit. While no contrast between the metal oxide and the substrate is visible in secondary electron SEM image due to the thinness of the film and the voltage used (15 kV, 6 kV), the ZrO_2 line appears in bright contrast in backscattering electron (BSE) SEM imaging (Figure 4a). Smooth lateral edges are noted for ZrO_2 (Figure 4a) in contrast with TiO_2 that displays a sharp EDS profile (Figure S3). The accurate localization of Titanium oxide is confirmed by X-ray photoelectron spectroscopy (XPS) linescans (Figure 4b). No Ti element is detected outside the deposit. Using triaxial nozzle with an outlet for a single precursor as injection head, a process of localized atomic layer deposition, called LOCALD, is thus demonstrated. Lateral resolution in the millimeter range is endorsed. Less than 2 mm resolution is established for ZrO_2 (Figure 4a) while ~2.7 mm is determined for TiO_2 localized SALD (Figure 4b). The difference in lateral resolution and in form factor is related to the deposition parameters that are established depending on the metal source.[53] The chosen deposition parameters like exhaust speed and substrate-head distance play a crucial role as they directly impact the distribution of the precursor flux on the surface and the eventual precursor intermixing.[54,62,63] It should be mentioned that precursor gas separation here might be not always optimal due to slight head tilt.

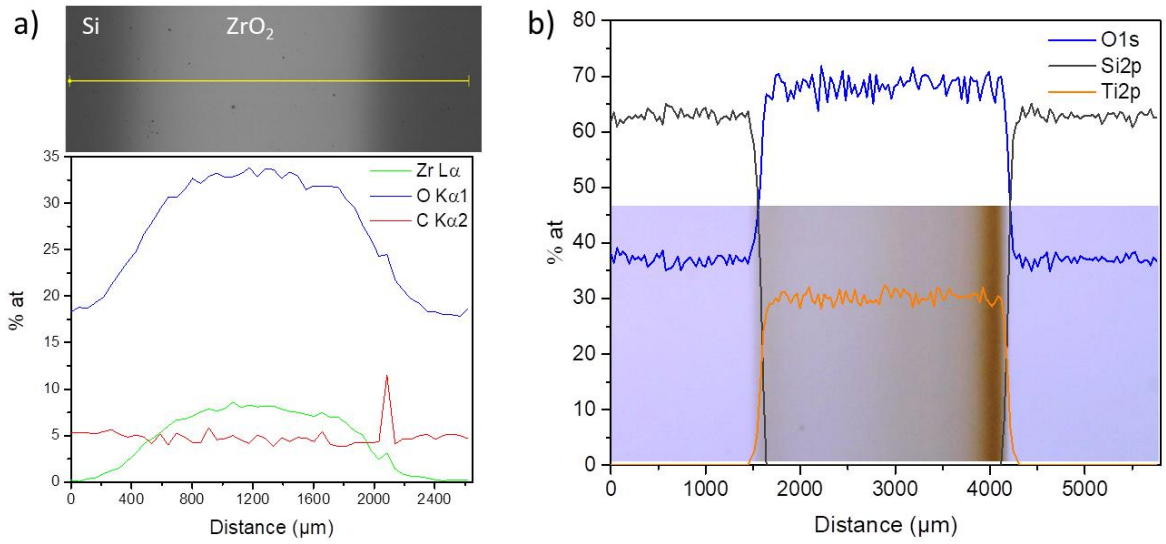

Figure 4. a) BSE SEM image of ZrO_2 line on Si and its corresponding EDS line profile. The ZrO_2 thickness is 54 nm. b) XPS linescans recorded along the width of 24 nm thick TiO_2 deposit on Si wafer.

Limited by the diameter of the precursor outlet, the lateral size of the deposit is between the inner diameter of the precursor outlet and the one of the exhaust. Controlling the dimension of the reactant outlet, thanks to an easily tunable head, and the deposition parameters permits adjusting the lateral resolution in a reversible manner. As proof of concept, an elongated glass capillary with a diameter of about 450 µm is fixed inside the inner needle to reduce its size (Figure 5). A sub-millimeter resolution (from 900 µm down to 500 µm) is then obtained as evidenced in Figure 5. Resolved TiO_2 grids with 1 mm pitch are successfully fabricated. The proposed LOCALD approach is highly promising to achieve patterns with tunable resolution down to sub-millimeter and even to micrometer range, by simple and reversible modification of the precursor outlet. It should be mentioned that the spatial resolution obtained here is greater than that previously reported using micro-plasma printer[52] and SALD pen.[53]

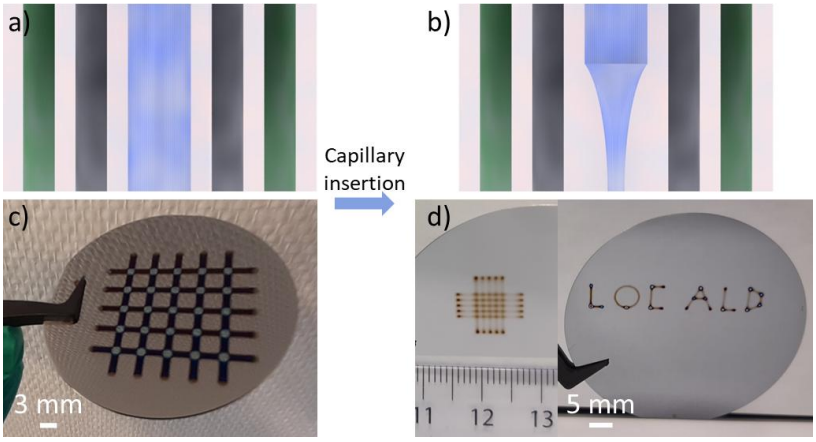

Figure 5. a-b) Scheme of the triaxial nozzle and examples of c) ZrO_2 grid and d) TiO_2 grid and text patterns on 2" Si wafers obtained as a function of the inner diameter. Distance between two neighboring and parallel lines of the c) ZrO_2 and d) TiO_2 grid is 5 mm and 1 mm, respectively. b) Introducing glass capillary permits to reduce and tune the

inner needle diameter and thus the lateral resolution. After needle modification, d) photographs of TiO_2 patterns on 2" Si wafers reveal a lateral resolution of hundreds µm.

A multi-oxide pattern can also be achieved using this set-up, demonstrating its versatility. As an example, two lines of ZrO_2 perpendicular to ones of TiO_2 are efficiently realized (Figure 6). Stack of both oxides is obtained at the crossing point as shown by the EDS spectrum (Figure 6b), recorded from a full BSE SEM image of the intersection. The presence of both Ti and Zr elements is confirmed; the observed Si and Sn elements arise from the substrate. The corresponding EDS maps (Figure 6c, S4) evidence the distribution in line of Zr and Ti. It should be mentioned here that the scanned area does not include the full width of the TiO_2 line.

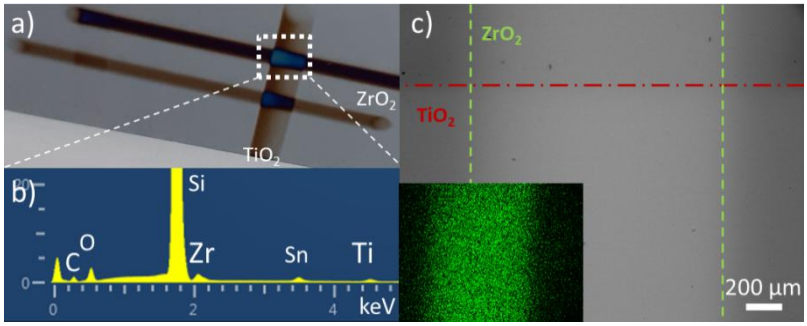

Figure 6. a) Photograph of ZrO_2-TiO_2 patterns deposited on Si wafer, b) EDS spectrum recorded from the intersection of both oxide lines, highlighted with the dotted white square in a). c) Corresponding BSE SEM image, green and orange dotted lines point at the position of ZrO_2 and TiO_2 lines, respectively. Only part of the titania line is visible on the image. In the inset, the corresponding EDS map, recorded at 15 kV, confirms the horizontal distribution of Zr element.

Various patterns with accurate control of the composition, thickness, size and localization are successfully achieved on flat substrates with tunable spatial resolution. However, conformal and uniform coating on high aspect ratio supports might be challenging using SALD[29,35,40,64] especially at atmospheric pressure, due to precursor supply and diffusion.[64,65] To study the conformability of the LOCALD technique, deposition on micro- and nano-textured supports, like patterned substrates (Figure S5) and nanostructures, is then investigated. Uniform and highly conformal TiO_2 and ZrO_2 LOCALD layers are successfully formed on SiO_2-Si patterned substrate. As visible in Figure 7a, ZrO_2 that appears in bright contrast follows perfectly the step topography of the support. Conformal TiO_2 coating is also identified on 1 µm diameter-polymer fibers electrospun on Si wafer (Figure S6). These results confirm the possibility to homogenously coat non-planar surfaces using the LOCALD approach, in agreement with previous SALD works on comparable structured substrates.[31,37,66,67] In particular, Muñoz-Rojas' group reported conformal deposition of ZnO and Al doped-ZnO on, respectively, textured Si[66] and ZnO nanowires deposited on Si wafer[68,69] using an open-air atmospheric pressure SALD reactor. Nevertheless, LOCALD on higher aspect ratio substrates such as black silicon reveals less homogeneity in depth with poor step coverage. SEM and EDS characterizations (Figure 7 and S7) show that SALD is effective only on the first part of the 40 µm long pillars. A dense oxide film visible in bright contrast (Figure 7b) is formed along the first top 800 nm - 1 µm as shown in side view SEM images (Figures 7c, d and S7). EDS Ti profile (Figure S7a) and Zr map (inset in Figure 7d) confirm the limited penetration into the black silicon

structure. Presumably using a longer exposure time could improve the diffusion depth of the precursor.[34,35] Therefore different substrate velocities are studied to modulate the exposure time; decreasing the speed resulting in longer precursor exposure time. In the range from 10 to 60 mm.s^{-1} no noticeable change in step coverage is observed. The low conformability could be attributed to insufficient precursor partial pressure and/or precursor supply.[28,65] Nonetheless, selective coverage of the top part of the structure could be advantageous as the main edges of the structure are preserved. It consists of a kind topological area selective deposition,[70] as observed with electron-enhanced ALD.[71,72] A second order of control seems thus accessible in this case, despite no further investigations are presented here as it is out of the scope of the present work.

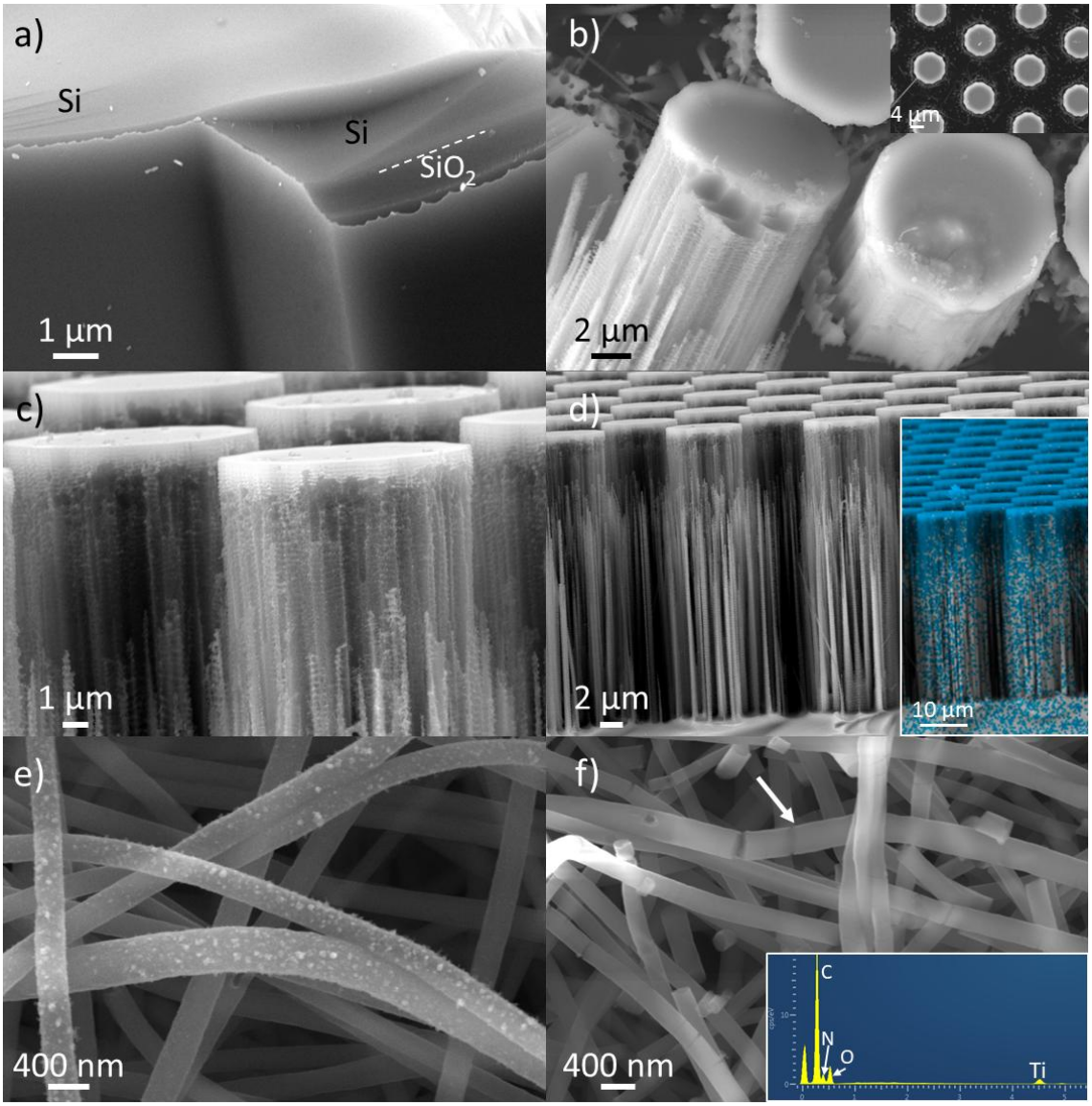

Figure 7. SEM images of a-e) ZrO_2 and f) TiO_2 lines deposited on three different micro- and nano-architectured substrates. a) SEM micrograph recorded on the edge of fractured SiO_2-Si patterned substrate after 400 SALD cycles reveals the conformal ZrO_2 coating (in bright contrast). The patterned 736 nm SiO_2-Si substrate (see guide lines) displays steps around 3 µm high. b) Top and c, d) side views of ZrO_2-coated black Si after 400 SALD cycles with

velocity of 20 mm.s^{-1} and 10 mm.s^{-1}, respectively. The deposition, visible in bright contrast, occurs on the top 800 nm-1st micrometer of the structure. Inset in d) Zr elemental EDS mapping confirms the coating on the first part only of the black Si support. Note: due to the sample fracture, Zr signal collected from the bottom may arise from both noise and small cutting fragments, on the edge. e) SEM image of PAN fibers after ZrO_2 SALD shows particles around the fibers, in addition to the continuous layer evidenced in Figure S7. On the opposite, f) SEM image recorded from TiO_2 coated PAN fibers reveals homogeneous deposition around the polymer. EDS spectrum, in the inset, confirms the presence of Ti element. White arrows point at cracks in the coating that are attributed to sample manipulation.

TiO_2 coating on unwoven polyacrylonitrile (PAN) fibers reveals to be smooth, continuous and uniform along the fibers (Figure 7f), although limited penetration depth into the core mat is noted. As for black silicon, the metal precursor does not diffuse through the entire mat thickness; no deposit is observed on the back of the fibrous support. Atmospheric pressure SALD on textile is challenging and requires specific design indeed.[73] Regarding LOCALD of ZrO_2 pattern on PAN textile, particles are formed on the upper fibers in addition to continuous layer, as evidenced in Figure 7f and Figure S7. It can be attributed to unwanted gas-phase reaction. As the mat surface is wavy, the distance between the support and the injection head is not constant over the displacement length. Such gap variation can be responsible for the CVD phenomenon. The latter is not observed in the case of TiO_2 deposition due to higher nitrogen fluxes that are used compared to the one of ZrO_2 deposition, preventing Ti precursor/air mixing.

Conclusions

In summary, maskless deposition of TiO_2 and ZrO_2 patterns is successfully achieved using an open-air SALD reactor with an injection head made of three concentric nozzles. Although the reactor design is very simple without a co-reactant outlet as water from the surrounding atmosphere is being used, SALD characteristics are still demonstrated. In particular, the linear dependence of the deposited thickness with the number of cycles is verified. Even though on very high aspect ratio substrates poor step coverage is observed, deposition on flat and structured supports reveals highly uniform and homogenous. Complex oxide patterns with thickness ranging from tens to hundreds of nanometers are then successfully achieved with z resolution at the nanoscale and lateral resolution easily tuned from millimeters to hundreds of micrometers range by reversible tuning the central outlet diameter. The same injection head is used independently of the targeted resolution, at the opposite of the previously reported SALD-pen, making the proposed approach, named LOCALD, highly versatile. Direct patterning of various metal oxides with different lateral sizes is thus easily accessible. Even though only oxides have been reported here, other types of materials as nitrides can be envisaged under a controlled atmosphere. LOCALD is thus certainly of interest in the nanofabrication industry. In particular, being an open-air approach, it can be compatible with roll-to-roll process.

Experimental Methods

Localized depositions were performed using a homemade atmospheric spatial atomic layer deposition set-up (Figure 1). The SALD injection nozzle consists of three concentric needles of 6G, 10G and 14G diameters, respectively. Only one precursor outlet is present, the co-reactant being water, naturally present in the surrounding atmosphere. The inner needle is connected to a bubbler containing the metal precursor. The intermediate and outer needles correspond, respectively, to the exhaust and the inert gas

outlet. Such a configuration allows miniaturizing the head and thus the localization of the deposit. The lateral resolution is easily tuned from mm to µm range in a versatile manner by inserting an elongated glass capillary (Figure 5) with the desired diameter into the central needle and glued with PMMA.

TiO_2 and ZrO_2 were deposited from, respectively, Titanium tetra-isopropoxide (TTIP, Sigma Aldrich) and Zirconium tert-butoxide (ZTB, STREM) maintained at 50 °C and 30-40 °C, while N_2 is used as the carrier and protective/purging gas. Water contained in relative humidity of the surrounding atmosphere was used as co-reactant like schematized in Figure 1. Depositions took place at 150 °C with N_2 protective flow from 15 to 200 sccm. The flow of N_2 used as carrier gas was varied in the range of 25-200 sccm and of 15-50 sccm for TTIP and ZTB, respectively. The exhaust speed, adjusted thanks to a rotameter, was fixed at 800 sccm. ZrO_2 was also deposited at 200 °C to study the influence of the substrate temperature on the film crystallinity. Flat substrates as silicon wafer with native oxide, glass and FTO slides, TA6V, Cu and Aluminum foils as well as structured supports like Si pillar (black silicon), SiO_2-Si patterned wafer and PAN fiber mats stabilized at 280 °C were used. The substrate, hold on an XY plate (Planar DL 100-XY-E1-PL3-TAS), from Aerotech, moved repetitively under the injection head with a velocity of 20 mm/s. Displacement of the stage is controlled by the software "*Ensemble Configuration Manager/Ensemble Motion Composer*" from Aerotech. The patterns are coded using "*AeroBasic"*. The gap between the substrate and the head was fixed and kept constant at 300 µm and 150 µm during the deposition of TiO_2 and ZrO_2, respectively.

Deposition of TiO_2 with increased lateral resolution using a capillary requires adjusting the parameters. TTIP was thus kept at 90-100 °C to raise the precursor concentration. Fluxes of N_2 carrier and protective gases as well as the exhaust speed were, respectively, optimized at 3-5 sccm, 30-50 sccm and 1240 sccm. Velocity of the stage was set at 40 mm/s.

The thickness of deposited films was measured by ellipsometry spectroscopy using a Sopra GES-5E spectrometer at an incidence angle of 70°. Data fit was realized with the "WinElli_II" software using Cauchy dispersion law. Optical observations of the deposits were realized using a BX60 Olympus microscope equipped with a CCD camera. Surface morphology and elemental composition of the oxide-coated materials were evaluated by scanning electron microscopy and energy-dispersive X-ray spectroscopy using a Zeiss Merlin VP compact microscope operated at 15 and 6 kV and equipped with an SDD OXFORD X-Max EDXS detector. Samples were prepared without any coating. Surface topography of TiO_2 and ZrO_2-coated Si wafer was characterized by AFM using a CSI-Nano Observer microscope operating in tapping mode. XRD patterns were recorded from TiO_2– and ZrO_2–coated Si samples with a PANalytical X'Pert Pro MPD diffractometer (CuKα radiation; λ = 1.5406 Å at 40 kV and 30 mA) to evaluate the crystallinity of the oxides. XPS was performed, using a THERMO K-alpha+ spectrometer with Al Kα monochromatism radiation and analyzed diameter of 30µm. Linescans were realized along several millimeters.

Associated content

Supporting Information

The Supporting Information is available free of charge *via* the Internet at http://pubs.acs.org. It includes: graphs of TiO_2 and ZrO_2 saturation curves as a function of the N_2 protective flow; AFM and SEM images

of TiO_2 and ZrO_2 lines deposited on Si wafer; Ti EDS profile from one edge of a 24 nm TiO_2 line deposited on Si; EDS map of Ti element; SEM images of the structured bare supports used; EDS line profile of Ti and C elements recorded on a polyethersulfone electrospun on Si wafer after 1000 TiO_2 LOCALD cycles; SEM images of TiO_2 and ZrO_2 deposited on black silicon and PAN fibers.

Author information

Corresponding Author

catherine.marichy@univ-lyon1.fr

Author Contributions

All authors have given approval to the final version of the manuscript.

Conflict of Interest

There are no conflicts of interest to declare.

Acknowledgments

The authors thank the "Centre Technologique des Microstructures", CTμ, (Université Lyon 1), for providing access to the SEM. "Science et surface" is acknowledged for the XPS characterization. The authors warmly thank J. Jose, M. Maillard and X. Jaurand for their fruitful advices and technical help. They also acknowledge L. Auvray for his help on AFM and G. Sala for mechanical engineering. Finally, a special thank is addressed to P. Poncharal from the "Institut Lumière Matière" lab for providing the glass capillaries.

References

(1) Aghajani, S.; Accardo, A.; Tichem, M. Tunable Photoluminescence and SERS Behaviour of Additively Manufactured Au Nanoparticle Patterns. *RSC Adv.* **2021**, *11* (28), 16849–16859. https://doi.org/10.1039/D1RA02266K.

(2) Graddage, N.; Chu, T.-Y.; Ding, H.; Py, C.; Dadvand, A.; Tao, Y. Inkjet Printed Thin and Uniform Dielectrics for Capacitors and Organic Thin Film Transistors Enabled by the Coffee Ring Effect. *Organic Electronics* **2016**, *29*, 114–119. https://doi.org/10.1016/j.orgel.2015.11.039.

(3) Hou, Z.; Lu, H.; Li, Y.; Yang, L.; Gao, Y. Direct Ink Writing of Materials for Electronics-Related Applications: A Mini Review. *FRONTIERS IN MATERIALS* **2021**, *8*. https://doi.org/10.3389/fmats.2021.647229.

(4) Tagliaferri, S.; Panagiotopoulos, A.; Mattevi, C. Direct Ink Writing of Energy Materials. *Mater. Adv.* **2021**, *2* (2), 540–563. https://doi.org/10.1039/D0MA00753F.

(5) Alberto Pique; David W. Weir; Peter K. Wu; Bhanu Pratap; Craig B. Arnold; Bradley R. Ringeisen; Robert Andrew McGill; Raymond C. Y. Auyeung; Richard A. Kant; Douglas B. Chrisey. Direct-Write of Sensor Devices by a Laser Forward Transfer Technique; 2002; Vol. 4637.

(6) Mathews, S. A.; Beniam, I.; Charipar, N.; Piqué, A. Laser Induced Forward Transfer (Lift) for Direct-Write Fabrication and Assembly of Microelectronics. *ICALEO* **2015**, *2015* (1), 9–13. https://doi.org/10.2351/1.5063251.

(7) Sarobol, P.; Cook, A.; Clem, P. G.; Keicher, D.; Hirschfeld, D.; Hall, A. C.; Bell, N. S. Additive Manufacturing of Hybrid Circuits. *Annu. Rev. Mater. Res.* **2016**, *46* (1), 41–62. https://doi.org/10.1146/annurev-matsci-070115-031632.
(8) Duty, C.; Jean, D.; Lackey, W. J. Laser Chemical Vapour Deposition: Materials, Modelling, and Process Control. *null* **2001**, *46* (6), 271–287. https://doi.org/10.1179/095066001771048727.
(9) Longo, D. M.; Hull, R. Direct Focused Ion Beam Writing of Printheads for Pattern Transfer Utilizing Microcontact Printing. *MRS Online Proceedings Library* **2000**, *624* (1), 157–162. https://doi.org/10.1557/PROC-624-157.
(10) Gavagnin, M.; Wanzenboeck, H. D.; Shawrav, M. M.; Belic, D.; Wachter, S.; Waid, S.; Stoeger–Pollach, M.; Bertagnolli, E. Focused Electron Beam-Induced CVD of Iron: A Practical Guide for Direct Writing. *Chemical Vapor Deposition* **2014**, *20* (7-8–9), 243–250. https://doi.org/10.1002/cvde.201407118.
(11) Li, P.; Chen, S.; Dai, H.; Yang, Z.; Chen, Z.; Wang, Y.; Chen, Y.; Peng, W.; Shan, W.; Duan, H. Recent Advances in Focused Ion Beam Nanofabrication for Nanostructures and Devices: Fundamentals and Applications. *NANOSCALE* **2021**, *13* (3), 1529–1565. https://doi.org/10.1039/d0nr07539f.
(12) Wallenberger, F. T.; Nordine, P. C.; Boman, M. Inorganic Fibers and Microstructures Directly from the Vapor Phase. *Composites Science and Technology* **1994**, *51* (2), 193–212. https://doi.org/10.1016/0266-3538(94)90190-2.
(13) Skoog, S. A.; Nguyen, A. K.; Kumar, G.; Zheng, J.; Goering, P. L.; Koroleva, A.; Chichkov, B. N.; Narayan, R. J. Two-Photon Polymerization of 3-D Zirconium Oxide Hybrid Scaffolds for Long-Term Stem Cell Growth. *Biointerphases* **2014**, *9* (2), 029014. https://doi.org/10.1116/1.4873688.
(14) Desponds, A.; Banyasz, A.; Montagnac, G.; Andraud, C.; Baldeck, P.; Parola, S. Microfabrication by Two-Photon Lithography, and Characterization, of SiO2/TiO2 Based Hybrid and Ceramic Microstructures. *Journal of Sol-Gel Science and Technology* **2020**, *95* (3), 733–745. https://doi.org/10.1007/s10971-020-05355-3.
(15) Martínez, E. D.; Prado, A.; Gonzalez, M.; Anguiano, S.; Tosi, L.; Salazar Alarcón, L.; Pastoriza, H. Recent Advances on Nanocomposite Resists With Design Functionality for Lithographic Microfabrication. *Frontiers in Materials* **2021**, *8*, 16. https://doi.org/10.3389/fmats.2021.629792.
(16) Oh, D.; Jeong, H.; Kim, J.; Kim, Y.; Kim, I.; Ok, J.; Rho, J. Top-down Nanofabrication Approaches toward Single-Digit-Nanometer Scale Structures. *JOURNAL OF MECHANICAL SCIENCE AND TECHNOLOGY* **2021**, *35* (3), 837–859. https://doi.org/10.1007/s12206-021-0243-7.
(17) Oh, D. K.; Lee, T.; Ko, B.; Badloe, T.; Ok, J. G.; Rho, J. Nanoimprint Lithography for High-Throughput Fabrication of Metasurfaces. *Frontiers of Optoelectronics* **2021**. https://doi.org/10.1007/s12200-021-1121-8.
(18) Shen, J.; Sun, W.; Liu, D.; Schaus, T.; Yin, P. Three-Dimensional Nanolithography Guided by DNA Modular Epitaxy. *Nature Materials* **2021**, *20* (5), 683–690. https://doi.org/10.1038/s41563-021-00930-7.
(19) George, S. M. Atomic Layer Deposition: An Overview. *Chemical Reviews* **2010**, *110* (1), 111–131. https://doi.org/10.1021/cr900056b.
(20) Hwang, C. S. Atomic Layer Deposition for Microelectronic Applications. In *Atomic Layer Deposition of Nanostructured Materials*; Wiley-VCH, 2011; p 161.
(21) Marichy, C.; Bechelany, M.; Pinna, N. Atomic Layer Deposition of Nanostructured Materials for Energy and Environmental Applications. *Advanced Materials* **2012**, *24* (8), 1017–1032. https://doi.org/10.1002/adma.201104129.
(22) Knez, M.; Nielsch, K.; Niinistö, L. Synthesis and Surface Engineering of Complex Nanostructures by Atomic Layer Deposition. *Advanced Materials* **2007**, *19* (21), 3425–3438. https://doi.org/10.1002/adma.200700079.

(23) Mackus, A. J. M.; Bol, A. A.; Kessels, W. M. M. The Use of Atomic Layer Deposition in Advanced Nanopatterning. *Nanoscale* **2014**, *6* (19), 10941–10960. https://doi.org/10.1039/C4NR01954G.
(24) Parsons, G. N.; Clark, R. D. Area-Selective Deposition: Fundamentals, Applications, and Future Outlook. *Chem. Mater.* **2020**, *32* (12), 4920–4953. https://doi.org/10.1021/acs.chemmater.0c00722.
(25) Suntola T.; Antson J. METHOD FOR PRODUCING COMPOUND THIN FILMS. US Patent 4,058,430, 1977.
(26) Suntola, T.; Pakkala, A. J.; Lindfors, S. G. Apparatus for Performing Growth of Compound Thin Films. US patent 4389973, 1983.
(27) (Erwin) Kessels, W. M. M.; Putkonen, M. Advanced Process Technologies: Plasma, Direct-Write, Atmospheric Pressure, and Roll-to-Roll ALD. *MRS Bulletin* **2011**, *36* (11), 907–913. https://doi.org/10.1557/mrs.2011.239.
(28) Muñoz-Rojas, D.; Maindron, T.; Esteve, A.; Piallat, F.; Kools, J. C. S.; Decams, J.-M. Speeding up the Unique Assets of Atomic Layer Deposition. *Materials Today Chemistry* **2019**, *12*, 96–120. https://doi.org/10.1016/j.mtchem.2018.11.013.
(29) Musselman, K. P.; Uzoma, C. F.; Miller, M. S. Nanomanufacturing: High-Throughput, Cost-Effective Deposition of Atomic Scale Thin Films via Atmospheric Pressure Spatial Atomic Layer Deposition. *Chem. Mater.* **2016**, *28* (23), 8443–8452. https://doi.org/10.1021/acs.chemmater.6b03077.
(30) Poodt, P.; Cameron, D. C.; Dickey, E.; George, S. M.; Kuznetsov, V.; Parsons, G. N.; Roozeboom, F.; Sundaram, G.; Vermeer, A. Spatial Atomic Layer Deposition: A Route towards Further Industrialization of Atomic Layer Deposition. *Journal of Vacuum Science & Technology A* **2011**, *30* (1), 010802. https://doi.org/10.1116/1.3670745.
(31) Hoye, R. L. Z.; MacManus-Driscoll, J. L. Atmospheric Pressure Spatial Atomic Layer Deposited Metal Oxides for Thin Film Solar Cells. In *Advanced Micro- and Nanomaterials for Photovoltaics*; Elsevier, 2019; pp 245–277. https://doi.org/10.1016/B978-0-12-814501-2.00010-4.
(32) van Ommen, J. R.; Kooijman, D.; Niet, M. de; Talebi, M.; Goulas, A. Continuous Production of Nanostructured Particles Using Spatial Atomic Layer Deposition. *Journal of Vacuum Science & Technology A* **2015**, *33* (2), 021513. https://doi.org/10.1116/1.4905725.
(33) Choi, H.; Shin, S.; Jeon, H.; Choi, Y.; Kim, J.; Kim, S.; Chung, S. C.; Oh, K. Fast Spatial Atomic Layer Deposition of Al2O3 at Low Temperature (<100 °C) as a Gas Permeation Barrier for Flexible Organic Light-Emitting Diode Displays. *Journal of Vacuum Science & Technology A* **2015**, *34* (1), 01A121. https://doi.org/10.1116/1.4934752.
(34) Yersak, A. S.; Sharma, K.; Wallas, J. M.; Dameron, A. A.; Li, X.; Yang, Y.; Hurst, K. E.; Ban, C.; Tenent, R. C.; George, S. M. Spatial Atomic Layer Deposition for Coating Flexible Porous Li-Ion Battery Electrodes. *Journal of Vacuum Science & Technology A* **2018**, *36* (1), 01A123. https://doi.org/10.1116/1.5006670.
(35) Sharma, K.; Routkevitch, D.; Varaksa, N.; George, S. M. Spatial Atomic Layer Deposition on Flexible Porous Substrates: ZnO on Anodic Aluminum Oxide Films and Al2O3 on Li Ion Battery Electrodes. *Journal of Vacuum Science & Technology A* **2016**, *34* (1), 01A146. https://doi.org/10.1116/1.4937728.
(36) Hoye, R. L. Z.; Muñoz-Rojas, D.; Nelson, S. F.; Illiberi, A.; Poodt, P.; Roozeboom, F.; MacManus-Driscoll, J. L. Research Update: Atmospheric Pressure Spatial Atomic Layer Deposition of ZnO Thin Films: Reactors, Doping, and Devices. *APL Materials* **2015**, *3* (4), 040701. https://doi.org/10.1063/1.4916525.
(37) Musselman, K. P.; Muñoz-Rojas, D.; Hoye, R. L. Z.; Sun, H.; Sahonta, S.-L.; Croft, E.; Böhm, M. L.; Ducati, C.; MacManus-Driscoll, J. L. Rapid Open-Air Deposition of Uniform, Nanoscale, Functional Coatings on Nanorod Arrays. *Nanoscale Horiz.* **2017**, *2* (2), 110–117. https://doi.org/10.1039/C6NH00197A.

(38) Levy, D. H.; Freeman, D.; Nelson, S. F.; Cowdery-Corvan, P. J.; Irving, L. M. Stable ZnO Thin Film Transistors by Fast Open Air Atomic Layer Deposition. *Appl. Phys. Lett.* **2008**, *92* (19), 192101. https://doi.org/10.1063/1.2924768.
(39) Cowdery-Corvan, P. J.; Levy, D. H.; Nelson, S. F.; Freeman, D. C.; Pawlik, T. D. Process for Atomic Layer Deposition. US Patent 2008/O182358A1, 2008.
(40) Muñoz-Rojas, D.; MacManus-Driscoll, J. Spatial Atmospheric Atomic Layer Deposition: A New Laboratory and Industrial Tool for Low-Cost Photovoltaics. *Mater. Horiz.* **2014**, *1* (3), 314–320. https://doi.org/10.1039/C3MH00136A.
(41) Hoye, R. L. Z.; Muñoz-Rojas, D.; Musselman, K. P.; Vaynzof, Y.; MacManus-Driscoll, J. L. Synthesis and Modeling of Uniform Complex Metal Oxides by Close-Proximity Atmospheric Pressure Chemical Vapor Deposition. *ACS Appl. Mater. Interfaces* **2015**, *7* (20), 10684–10694. https://doi.org/10.1021/am5073589.
(42) Poodt, P.; Kniknie, B.; Branca, A.; Winands, H.; Roozeboom, F. Patterned Deposition by Plasma Enhanced Spatial Atomic Layer Deposition. *physica status solidi (RRL) – Rapid Research Letters* **2011**, *5* (4), 165–167. https://doi.org/10.1002/pssr.201004542.
(43) Aghaee, M.; Maydannik, P. S.; Johansson, P.; Kuusipalo, J.; Creatore, M.; Homola, T.; Cameron, D. C. Low Temperature Temporal and Spatial Atomic Layer Deposition of TiO2 Films. *Journal of Vacuum Science & Technology A* **2015**, *33* (4), 041512. https://doi.org/10.1116/1.4922588.
(44) Muñoz-Rojas, D.; Nguyen, V. H.; Masse de la Huerta, C.; Aghazadehchors, S.; Jiménez, C.; Bellet, D. Spatial Atomic Layer Deposition (SALD), an Emerging Tool for Energy Materials. Application to New-Generation Photovoltaic Devices and Transparent Conductive Materials. *Comptes Rendus Physique* **2017**, *18* (7), 391–400. https://doi.org/10.1016/j.crhy.2017.09.004.
(45) Hoye, R. L. Z.; Muñoz-Rojas, D.; Iza, D. C.; Musselman, K. P.; MacManus-Driscoll, J. L. High Performance Inverted Bulk Heterojunction Solar Cells by Incorporation of Dense, Thin ZnO Layers Made Using Atmospheric Atomic Layer Deposition. *Solar Energy Materials and Solar Cells* **2013**, *116*, 197–202. https://doi.org/10.1016/j.solmat.2013.04.020.
(46) Muñoz-Rojas, D.; Sun, H.; Iza, D. C.; Weickert, J.; Chen, L.; Wang, H.; Schmidt-Mende, L.; MacManus-Driscoll, J. L. High-Speed Atmospheric Atomic Layer Deposition of Ultra Thin Amorphous TiO2 Blocking Layers at 100 °C for Inverted Bulk Heterojunction Solar Cells. *Progress in Photovoltaics: Research and Applications* **2013**, *21* (4), 393–400. https://doi.org/10.1002/pip.2380.
(47) Poodt, P.; Lankhorst, A.; Roozeboom, F.; Spee, K.; Maas, D.; Vermeer, A. High-Speed Spatial Atomic-Layer Deposition of Aluminum Oxide Layers for Solar Cell Passivation. *Advanced Materials* **2010**, *22* (32), 3564–3567. https://doi.org/10.1002/adma.201000766.
(48) Maydannik, P. S.; Kääriäinen, T. O.; Lahtinen, K.; Cameron, D. C.; Söderlund, M.; Soininen, P.; Johansson, P.; Kuusipalo, J.; Moro, L.; Zeng, X. Roll-to-Roll Atomic Layer Deposition Process for Flexible Electronics Encapsulation Applications. *Journal of Vacuum Science & Technology A* **2014**, *32* (5), 051603. https://doi.org/10.1116/1.4893428.
(49) Nelson, S. F.; Ellinger, C. R.; Levy, D. H. Improving Yield and Performance in ZnO Thin-Film Transistors Made Using Selective Area Deposition. *ACS Appl. Mater. Interfaces* **2015**, *7* (4), 2754–2759. https://doi.org/10.1021/am5077638.
(50) Levy, D. H.; Nelson, S. F.; Freeman, D. Oxide Electronics by Spatial Atomic Layer Deposition. *J. Display Technol.* **2009**, *5* (12), 484–494.
(51) Ellinger, C. R.; Nelson, S. F. Design Freedom in Multilayer Thin-Film Devices. *ACS Appl. Mater. Interfaces* **2015**, *7* (8), 4675–4684. https://doi.org/10.1021/am508088p.
(52) Aghaee, M.; Verheyen, J.; Stevens, A. A. E.; Kessels, W. M. M.; Creatore, M. TiO2 Thin Film Patterns Prepared by Chemical Vapor Deposition and Atomic Layer Deposition Using an

Atmospheric Pressure Microplasma Printer. *Plasma Processes and Polymers* **2019**, *16* (12), 1900127. https://doi.org/10.1002/ppap.201900127.
(53) Masse de la Huerta, C. A.; Nguyen, V. H.; Sekkat, A.; Crivello, C.; Toldra-Reig, F.; Veiga, P. B.; Quessada, S.; Jimenez, C.; Muñoz-Rojas, D. Gas-Phase 3D Printing of Functional Materials. *Advanced Materials Technologies* **2020**, *5* (n/a), 2000657. https://doi.org/10.1002/admt.202000657.
(54) Masse de la Huerta, C.; Nguyen, V.; Dedulle, J.-M.; Bellet, D.; Jiménez, C.; Muñoz-Rojas, D. Influence of the Geometric Parameters on the Deposition Mode in Spatial Atomic Layer Deposition: A Novel Approach to Area-Selective Deposition. *Coatings* **2019**, *9* (1), 5. https://doi.org/10.3390/coatings9010005.
(55) Yersak, A. S.; Lee, Y. C.; Spencer, J. A.; Groner, M. D. Atmospheric Pressure Spatial Atomic Layer Deposition Web Coating with in Situ Monitoring of Film Thickness. *Journal of Vacuum Science & Technology A* **2014**, *32* (1), 01A130. https://doi.org/10.1116/1.4850176.
(56) Aarik, J.; Aidla, A.; Uustare, T.; Ritala, M.; Leskelä, M. Titanium Isopropoxide as a Precursor for Atomic Layer Deposition: Characterization of Titanium Dioxide Growth Process. *Applied Surface Science* **2000**, *161* (3–4), 385–395. https://doi.org/10.1016/S0169-4332(00)00274-9.
(57) Park, M. H.; Jang, Y. J.; Sung-Suh, H. M.; Sung, M. M. Selective Atomic Layer Deposition of Titanium Oxide on Patterned Self-Assembled Monolayers Formed by Microcontact Printing. *Langmuir* **2004**, *20* (6), 2257–2260. https://doi.org/10.1021/la035760c.
(58) Sinha, A.; Hess, D. W.; Henderson, C. L. Area Selective Atomic Layer Deposition of Titanium Dioxide: Effect of Precursor Chemistry. *Journal of Vacuum Science & Technology B: Microelectronics and Nanometer Structures Processing, Measurement, and Phenomena* **2006**, *24* (6), 2523–2532. https://doi.org/10.1116/1.2359728.
(59) Nakajima, A.; Kidera, T.; Ishii, H.; Yokoyama, S. Atomic-Layer Deposition of ZrO2 with a Si Nitride Barrier Layer. *Applied Physics Letters* **2002**, *81* (15), 2824–2826. https://doi.org/10.1063/1.1510584.
(60) Ishii, H.; Nakajima, A.; Yokoyama, S. Growth and Electrical Properties of Atomic-Layer Deposited ZrO2/Si-Nitride Stack Gate Dielectrics. *Journal of Applied Physics* **2004**, *95* (2), 536–542. https://doi.org/10.1063/1.1629773.
(61) Kukli, K.; Ritala, M.; Leskelä, M. Low-Temperature Deposition of Zirconium Oxide–Based Nanocrystalline Films by Alternate Supply of Zr[OC(CH3)3]4 and H2O. *Chemical Vapor Deposition* **2000**, *6* (6), 297–302. https://doi.org/10.1002/1521-3862(200011)6:6<297::AID-CVDE297>3.0.CO;2-8.
(62) Nguyen, V. H.; Sekkat, A.; Jiménez, C.; Muñoz, D.; Bellet, D.; Muñoz-Rojas, D. Impact of Precursor Exposure on Process Efficiency and Film Properties in Spatial Atomic Layer Deposition. *Chemical Engineering Journal* **2021**, *403*, 126234. https://doi.org/10.1016/j.cej.2020.126234.
(63) Ryan Fitzpatrick, P.; Gibbs, Z. M.; George, S. M. Evaluating Operating Conditions for Continuous Atmospheric Atomic Layer Deposition Using a Multiple Slit Gas Source Head. *Journal of Vacuum Science & Technology A* **2011**, *30* (1), 01A136. https://doi.org/10.1116/1.3664765.
(64) Moitzheim, S.; Balder, J. E.; Ritasalo, R.; Ek, S.; Poodt, P.; Unnikrishnan, S.; De Gendt, S.; Vereecken, P. M. Toward 3D Thin-Film Batteries: Optimal Current-Collector Design and Scalable Fabrication of TiO2 Thin-Film Electrodes. *ACS Appl. Energy Mater.* **2019**, *2* (3), 1774–1783. https://doi.org/10.1021/acsaem.8b01905.
(65) Poodt, P.; Mameli, A.; Schulpen, J.; Kessels, W. M. M. (Erwin); Roozeboom, F. Effect of Reactor Pressure on the Conformal Coating inside Porous Substrates by Atomic Layer Deposition. *Journal of Vacuum Science & Technology A* **2017**, *35* (2), 021502. https://doi.org/10.1116/1.4973350.
(66) Nguyen, V. H.; Resende, J.; Jiménez, C.; Deschanvres, J.-L.; Carroy, P.; Muñoz, D.; Bellet, D.; Muñoz-Rojas, D. Deposition of ZnO Based Thin Films by Atmospheric Pressure Spatial Atomic

Layer Deposition for Application in Solar Cells. *Journal of Renewable and Sustainable Energy* **2017**, *9* (2), 021203. https://doi.org/10.1063/1.4979822.

(67) Heikkinen, I. T. S.; Koutsourakis, G.; Virtanen, S.; Yli-Koski, M.; Wood, S.; Vähänissi, V.; Salmi, E.; Castro, F. A.; Savin, H. AlOx Surface Passivation of Black Silicon by Spatial ALD: Stability under Light Soaking and Damp Heat Exposure. *Journal of Vacuum Science & Technology A* **2020**, *38* (2), 022401. https://doi.org/10.1116/1.5133896.

(68) Nguyen, V. H.; Resende, J.; Papanastasiou, D. T.; Fontanals, N.; Jiménez, C.; Muñoz-Rojas, D.; Bellet, D. Low-Cost Fabrication of Flexible Transparent Electrodes Based on Al Doped ZnO and Silver Nanowire Nanocomposites: Impact of the Network Density. *Nanoscale* **2019**, *11* (25), 12097–12107. https://doi.org/10.1039/C9NR02664A.

(69) Morisot, F.; Zuliani, C.; Luque, J.; Ali, Z.; Mouis, M.; Nguyen, V. H.; Muñoz-Rojas, D.; Lourhzal, O.; Texier, M.; Cornelius, T. W.; Ternon, C. ZnO Based Nanowire Network for Gas Sensing Applications. *Mater. Res. Express* **2019**, *6* (8), 084004. https://doi.org/10.1088/2053-1591/ab1f60.

(70) Vallée, C.; Bonvalot, M.; Belahcen, S.; Yeghoyan, T.; Jaffal, M.; Vallat, R.; Chaker, A.; Lefèvre, G.; David, S.; Bsiesy, A.; Possémé, N.; Gassilloud, R.; Granier, A. Plasma Deposition—Impact of Ions in Plasma Enhanced Chemical Vapor Deposition, Plasma Enhanced Atomic Layer Deposition, and Applications to Area Selective Deposition. *Journal of Vacuum Science & Technology A* **2020**, *38* (3), 033007. https://doi.org/10.1116/1.5140841.

(71) Sprenger, J. K.; Sun, H.; Cavanagh, A. S.; Roshko, A.; Blanchard, P. T.; George, S. M. Electron-Enhanced Atomic Layer Deposition of Boron Nitride Thin Films at Room Temperature and 100 °C. *The Journal of Physical Chemistry C* **2018**, *122* (17), 9455–9464. https://doi.org/10.1021/acs.jpcc.8b00796.

(72) Sprenger, J. K.; Sun, H.; Cavanagh, A. S.; George, S. M. Electron-Enhanced Atomic Layer Deposition of Silicon Thin Films at Room Temperature. *Journal of Vacuum Science & Technology A* **2018**, *36* (1), 01A118. https://doi.org/10.1116/1.5006696.

(73) Mousa, M. B. M.; Ovental, J. S.; Brozena, A. H.; Oldham, C. J.; Parsons, G. N. Modeling and Experimental Demonstration of High-Throughput Flow-through Spatial Atomic Layer Deposition of Al2O3 Coatings on Textiles at Atmospheric Pressure. *Journal of Vacuum Science & Technology A* **2018**, *36* (3), 031517. https://doi.org/10.1116/1.5022077.

Table of Contents (TOC) graphic